Section III
Auroral Region

7

ULF Waves above the Nightside Auroral Oval during Substorm Onset

I. J. Rae[1] and C. E. J. Watt[2]

7.1. INTRODUCTION

Magnetohydrodynamic (MHD) waves propagating in Earth's magnetotail represent a fundamental method for the transfer of energy and momentum throughout the magnetosphere–ionosphere system. Rapid changes in magnetotail stresses are mediated between the magnetosphere and ionosphere via ultra-low-frequency (ULF) waves. A magnetotail dipolarization can be thought of as a compressional or rarefaction wave progressing outwards from the inner magnetosphere, and shear Alfvén waves carry the current that couples the magnetosphere to the ionosphere, creating current systems such as the substorm current wedge (SCW) as well as those currents responsible for generating the aurora.

Decades of research have shown the importance of ULF waves during substorms. In this chapter, we review historical ground-based observations of ULF waves tied to substorms, and highlight new research linking these ULF waves explicitly to substorm onset itself. Through the study of ground magnetic and auroral measurements by the next generation of closely spaced instrument arrays, it is possible to investigate much more deeply the physics operating at substorm onset and within the aurora itself.

7.2. WHAT IS A SUBSTORM?

As Vytenis Vasyliunas stated eloquently in 2012, a substorm is "an explosive phenomenon in the Earth's magnetosphere that dipolarizes the magnetic field and polarizes the scientific community." More seriously, this is an accurate but incomplete physical description of the substorm. Substorm onsets must include:

- auroral brightening and poleward expansion;
- an enhancement in the ionospheric current systems and formation of geomagnetic bays, which can be positive or negative depending on the latitude and local time of the observation;
- a dipolarization of the stretched nightside magnetic fields;
- ULF waves.

In this chapter, we focus on the role of ULF waves above the aurora and their role in substorm expansion phase onset. In the next section, we discuss the historical context.

7.2.1. Magnetic Bay Associated with Enhanced Auroral Currents

In 1747, Olaf Peter Hjorter and Anders Celsius discovered that auroral displays were also a magnetic phenomenon. By taking ~10,000 hourly measurements in a two-year period (i.e. over ~17,520 hours), these authors determined that the presence of the aurora was always accompanied by a deflection in the geomagnetic field.

Fast-forward two centuries to a winter's research in Alaska that provided the first observations of the links between the initial substorm brightening and large magnetic field deflections. *Heppner* [1954] discovered that the brightening of the most equatorward auroral arc in the pre-midnight sector (the arc that subsequently "breaks up") was concurrent with the sharp decrease in the north–south (H-) component of the ground magnetometers. Subsequently, this research was turned into a

[1]*Department of Space and Climate Physics, Mullard Space Science Laboratory, Holmbury St. Mary, Dorking, Surrey, UK*

[2]*Department of Meteorology, University of Reading, Earley Gate, Reading, UK*

Low-Frequency Waves in Space Plasmas, Geophysical Monograph 216, First Edition.
Edited by Andreas Keiling, Dong-Hun Lee, and Valery Nakariakov.

doctoral thesis and a Defence Research Board of Canada report [*Heppner*, 1958]. This report marks the first time that the changes in aurora and the changes in magnetic fields were scientifically linked.

7.2.2. The Substorm: An Auroral Brightening That Expands over the Sky

After another winter season's observing campaign (in Alaska, Russia, and Europe) *Syun-ichi Akasofu* determined that the substorm was a repeatable global phenomenon that could be classified into a series of well-defined events that describe an expansion phase and a recovery phase [*Akasofu*, 1964]. It was only later that *McPherron* [1970] added the key missing ingredient into the substorm paradigm; the storage of energy in the "growth phase." The nomenclature of the three substorm phases—growth, expansion, and recovery—persists to this day.

For the expansion phase, *Akasofu* [1964] classified a series of ~5 min intervals, where the initial interval encompassed the first auroral brightening that signifies auroral onset. If this auroral brightening did not progress poleward for more than a few minutes, it would be termed a "pseudo-breakup." Subsequently, *Akasofu and Kan* [1982] produced the definition of substorm onset that we use today: a substorm onset is "the moment when an auroral arc brightens suddenly and begins to advance poleward." We should caution that this "moment" can last of the order of minutes, since it pertains to an interval of growth in intensity of an auroral arc. Defining a unique onset time for a changing phenomenon that can take tens of seconds to evolve from dim to bright is an exercise in futility. Rather, in this chapter, we discuss the ULF physics during the few minutes surrounding the initiation of the substorm, linking magnetic and optical observations to show that ULF waves can provide a new insight into the physics of substorm onset.

7.2.3. ULF Waves, Invoked to Carry the Current

In the early 1960s, Jacobs [*Jacobs and Sinno*, 1960] and Saito [*Saito*, 1969, and references therein] and co-workers recognized that ULF waves were an integral part of substorm physics. These authors tied pulsations at many different frequencies, which were initially described phenomenologically using wildly different acronyms, to the formation of the large geomagnetic bay that develops during the expansion phase. Subsequently, different ULF wave bands have been studied during the interval that surrounds substorm onset, particularly using observations from ground-based magnetometry [e.g., *Olson and Rostoker*, 1975]. These associations have been studied repeatedly, using all manner of ground-based systems. But our understanding of how the substorm detonates is hampered by a lack of understanding of exactly how auroral, magnetic, and plasma features relate to one another. In the following sections, we show recent work demonstrating that the rapid auroral brightening of substorm expansion phase onset is intimately linked to growth of electromagnetic ULF waves, and that the spatial structuring of the aurora and growth characteristics of the magnetic pulsations display key aspects of the same substorm onset phenomenon; that is, the formation and evolution of a near-Earth magnetotail plasma instability.

7.2.4. Substorms and Repeatable ULF Wave Signatures

In the early 1960s, it was recognized that there was a plethora of classifications of magnetospheric micropulsations based on either frequency range [e.g., *Jacobs et al.*, 1963] or an attempted association with physical phenomena [e.g., *Matsushita*, 1963; *Saito*, 1969]. As a consequence, a committee was convened after the 13th International Union of Geodesy and Geophysics (IUGG), in order to re-classify ULF pulsations in a common form. *Jacobs et al.* [1964] brought together these classifications into a basic unified scheme that is still being adhered to today. Generally speaking, there are two accepted classes; pulsations with a continuous, regular character termed "Pc" and those with an irregular pattern, termed "Pi." It is generally accepted that Pi pulsations form the basis of most substorm-related ULF wave activity; there are many additional non–substorm-related ULF waves that also occur in the nightside magnetosphere and ionosphere (see review by *Keiling and Takahashi* [2011], and references therein). Here we also note that in 1964, the main aim of bringing the different classifications together was to *reduce* the terminology used by different groups to describe the same physical phenomena. It is telling that even the authors of this seminal paper had disagreements. *Jacobs et al.* [1964] emphasize that these classifications should evolve with time and understanding, stating that "[i]n any decisions on classification, some compromise is inevitable. Since the physical processes involved are not well understood, it is pointless to introduce a highly sophisticated scheme." Since we have significantly more understanding from the past 50 years of research, it now appears more appropriate to ditch this classification altogether in the context of substorm research, and broaden our analysis to consider the full spectrum of ULF waves.

7.2.5. Measuring ULF Waves Using Ground-Based Magnetometers

In order to accurately measure the variations in Earth's geomagnetic field across all relevant temporal scales, two separate magnetometer systems are required. Fluxgate magnetometers measure the absolute value of the magnetic field but their response typically drops off with

frequency above ~1 Hz. Search coil or induction coil magnetometers measure the variations in Earth's magnetic field (through Faraday's law). They can measure ULF waves up to 1 kHz, but their performance drops off as those frequencies decrease towards ~1 Hz. In general, fluxgate magnetometry is a more widely used and simpler system to deploy, whereas induction coil or search coil magnetometers are trickier and more expensive to deploy and maintain. However, both these systems provide excellent insight into the substorm, and we discuss the relevant literature in both high (>1 Hz) and low (<1 Hz) frequency bands below.

Geomagnetic micropulsations in ground magnetometer data [e.g., *Jacobs et al.*, 1964] accompany the large geomagnetic bay during the substorm expansion phase when the diversion of the cross-tail current occurs through the nighttime ionosphere [e.g., *McPherron et al.*, 1973].

Pi2 pulsations (40–150 s period as specified by *Jacobs et al.* [1964]) in ground magnetometer data can be used to determine the location of the substorm current wedge (SCW) and its large-scale upward and downward field-aligned current (FAC) elements. They are less useful for determining the precise onset time for the substorm, since expansion phase onset typically occurs over timescales tens of seconds, or less than a wave period (e.g., see reviews by *Petrukovich and Yahnin* [2006] and *Sibeck and Angelopoulos* [2008]). At and after substorm expansion phase onset, Pi2 ULF waves can be observed across a huge range of local times, including on the dayside, and hence are usually thought to be more of a global phenomenon. Pi2 pulsations can be observed with low temporal resolution fluxgate magnetometers (FGM) on the ground or in space with a cadence of 5–10 s or higher, and despite the low resolution, we can still extract significant physical meaning from the analysis of these time series (e.g., pure state filtering championed by *Samson* [1983]).

The study of Pi1 pulsations in the 1–40 s period range have concentrated on the shorter periods of Pi1 waves, in the 1–10 s period band characterized as Pi1B (Pi1 Broadband; *Bösinger* [1989]; *Lessard et al.* [2006]). This small period band is singled out presumably as a consequence of limitations in instrumentation as opposed to physical processes. The 1–10 s Pi1B pulsations are traditionally measured with search coil magnetometer (SCM) instrumentation, which is capable of producing higher cadence measurements. This is perhaps why *Jacobs et al.* [1964] mention that "[u]sually the period of Pi1 is quite small, seldom exceeding 20 sec." Given that available instrumentation some 50 years ago would not have been able to resolve the 10–40 s wave band particularly well, it is perhaps not surprising that these waves went largely ignored until recent technological advancements. Pi1B pulsations have been linked to auroral luminosity fluctuations [e.g., *Troitskaya*, 1961], cosmic noise absorption [e.g., *Heacock and Hunsucker*, 1977], and the occurrence of ionospheric currents [e.g., *Bösinger et al.*, 1981]. Specifically with regard to the substorm, enhancements in Pi1B pulsations have been observed to be co-located with the auroral location of substorm onset [e.g., *Bösinger and Yahnin*, 1987; *Arnoldy et al.*, 1987; *Bösinger*, 1989], leading *Bösinger and Yahnin* [1987] to propose "Pi1Bs for reliable timing (in) a large dense network." More recently, *Posch et al.* [2007] determined that Pi1B amplitudes show dramatic increases in the location of auroral onset and within the time window required to take a global auroral image. At locations away from the onset site, Pi1B amplitudes rapidly decrease.

Indeed, *Jacobs et al.* [1964] had already noted that there are further waves to be studied during substorm onset, since "… pulsations during a magnetic bay (Pb) may be expressed as Pb = Pi1 + Pi2 + Pc1," and so as early as the 1960s, it was recognized that we should be viewing the entire frequency spectrum and not just isolated frequency bands.

7.2.6. Relationship between ULF Waves and Substorm Onset: The Early Years

The currents flowing into the ionosphere are mediated by electromagnetic waves. However, it is difficult to isolate the signatures of magnetospheric ULF waves of any frequency in the auroral zone, where fluctuating ionospheric currents are the norm. Identifying the onset of a long-period ULF wave in a time series filled with noise cannot be achieved through visual inspection. The integrated ionospheric currents that provide variations in the ground-based magnetometer time series are inherently noisy, particularly in the auroral oval. Consequently, finding the first evidence of ULF wave activity above the noise level requires sophisticated data analysis to avoid introducing thresholding effects, or station-dependent results. In general, this means that the ground-based observation of magnetospheric ULF waves during substorm onset (by definition, a phenomenon that occurs in the auroral zone) has historically been performed from sub-auroral latitudes. Away from the rapidly fluctuating auroral zone, mid-latitude observations of Pi2 waves have been used to provide important and robust scientific results. The polarization characteristics of Pi2s can be used to determine the large-scale characteristics of the SCW, including defining the locations of the upward and downward field-aligned current (FAC) elements and the central meridian [e.g., *Lester et al.*, 1983, 1984].

During the past decade, the substorm community has developed several significant new capabilities and data-analysis techniques. The resulting scientific developments have led to a new understanding of the substorm detonation process. Although advanced time-series analysis such as pure state filtering has been around for decades [e.g., *Samson*, 1973], a combination of several factors has

allowed the analysis of ground-based ionospheric monitoring data to flourish and deliver much improved scientific data products. The Canadian Space Agency (CSA) Canadian Geospace Monitoring program [http://www.cgsm.ca/; now Geospace Observatory Canada] and the NASA THEMIS mission [*Angelopoulos*, 2008; *Russell et al.*, 2008; *Mende et al.*, 2008] have provided increased temporal cadence and spatial resolution of ground-based ionospheric instrumentation across the North American continent. Most importantly, this development has ensured that their hard-won data are freely shared within the scientific community. One of the most valuable aspects of the THEMIS mission was the promotion of existing and easy-to-use IDL software that provided scientists with quick and easy access to not only the THEMIS *in situ* and ground magnetometer and ASI data but also access to many other crucial datasets (i.e., ground magnetometer data from the CARISMA [*Mann et al.*, 2008], CANMOS, GIMA, and other ground magnetometer chains). These new capabilities, combined with innovative approaches to time-series analysis, have opened up a new window in substorm research.

Table 7.1 General advantages and disadvantages of using a discrete wavelet transform as compared to traditional discrete Fourier transform analysis.

Discrete Wavelet Transform (DWT)	Traditional Discrete Fourier Analysis
Tailoring of wavelet basis function to realistic ULF wave characteristics (e.g., impulsive)	Decomposed signal into a series of sine waves
Nonstationary time-series analysis possible	Valid only for stationary time-series analysis
Convolves well with signal, poorly with noise	Convolves well with signal, well with noise
Poor frequency resolution, but band-limited	Variable frequency resolution, not band-limited
Overlapping frequency bands	Discrete frequency bands
Excellent timing	Poor timing
Can provide uncertainties in timing	Does not provide uncertainties in timing

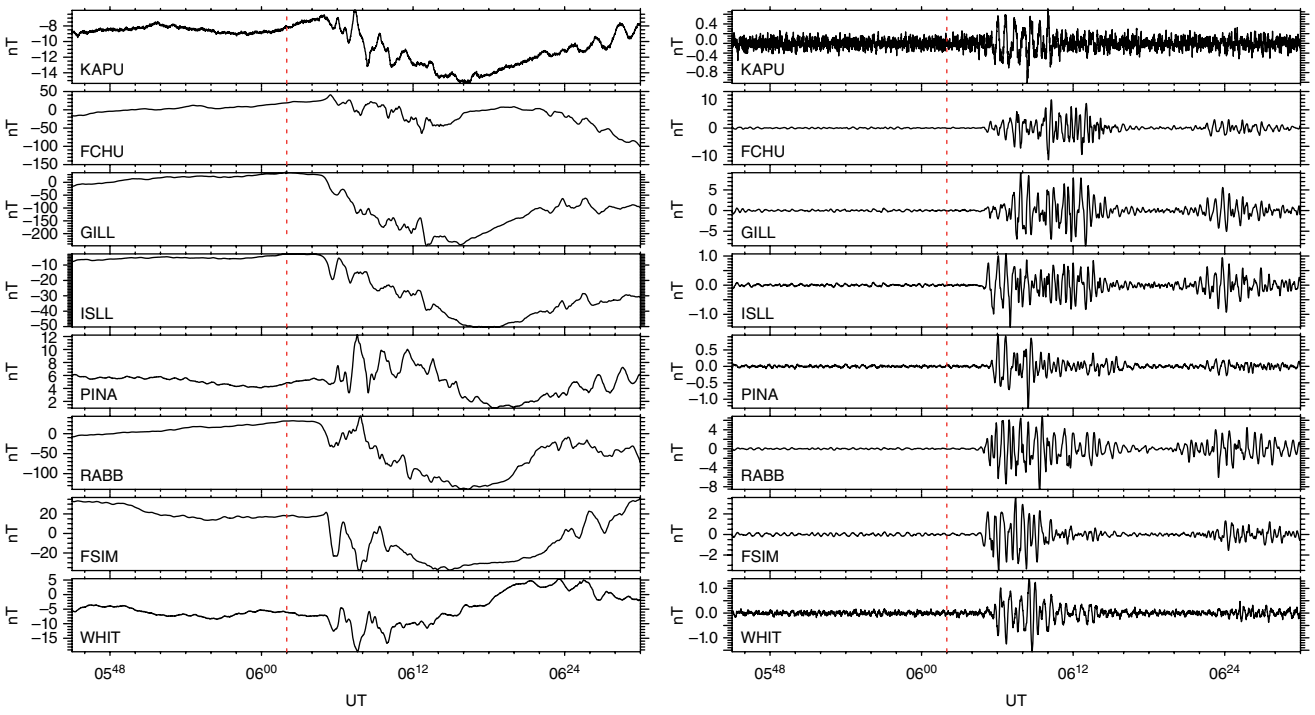

Figure 7.1 Selected CARISMA and THEMIS GMAG H-component ground magnetic fields observed between 0545–0630 UT on 1 November 2006: KAPU is eastern-most, FCHU-PINA are the "Churchill Line" and RABB-WHIT are arranged east–west. A small substorm, identified by a small (<280 nT) negative H-bay starting at ~0605 UT at GILL occurred in the Canadian sector (3rd panel from top on left hand side). Also visible in the right hand panel are the associated Pi1 waveforms clearly apparent in the ~10 min following expansion phase onset (for brevity, the Pi2 filtered signals are not shown here).

7.3. DISCOVERY OF A ULF WAVE EPICENTRE TO SUBSTORM ONSET

Fourier analysis is the initial "tool of choice" in many time-series analyses, but it is of limited use for a nonstationary time series (e.g., one where fluctuations grow or decay in amplitude with time, or where the time average of the dataset is not centred around zero). There are several robust methods that can be used to determine the characteristics of a nonstationary time series such as the ULF magnetic field traces observed in the auroral zone during substorms. These include the pure state filter [e.g., *Samson*, 1973], the Hilbert-Huang transform [e.g., *Kataoka et al.*, 2009], and wavelet analysis [e.g., *Nose et al.*, 1998; *Milling et al.*, 2008; *Murphy et al.*, 2009]. In wavelet analysis, a complete set of wavelet basis functions (i.e., a wavelet that covers the entire frequency and temporal spectrum) can be used to decompose a signal into wavelet coefficients (e.g., power) that are localized in time and band-limited in frequency. Furthermore, the defining characteristics of a particular ULF wave signal can be represented in the wavelet basis function chosen. For example, for impulsive, irregular ULF waves observed in the nightside ionosphere, the Meyer wavelet [*Meyer*, 1989] provides an excellent basis function that resembles an impulsive ULF wave (first chosen by *Nose et al.* [1998] and outlined further below). Table 7.1 displays a comparison between the features of a discrete wavelet transform, and the more traditional discrete Fourier analysis.

Milling et al. [2008] applied a discrete wavelet transform (DWT) analysis based on *Nose et al.* [1998] to study the entire ULF wave spectrum during this substorm measured by a significant number of spatially separated ground magnetometers from the CARISMA [*Mann et al.*, 2008] and THEMIS [*Russell et al.*, 2008] magnetometer chains. Figure 7.1 shows (left) H-component and (right) 1–40 s period band-pass Fourier-filtered ground magnetometer data from a series of stations from the CARISMA and THEMIS chains during a small substorm, where onset is marked by the dashed line. It is impossible to extract a well-defined onset time from the filtered time series as presented on the right of the figure.

The DWT analysis (using a Meyer wavelet) demonstrated that the first ULF wave band to rise above a predetermined band-specific noise threshold was the long-period Pi1/short-period Pi2 frequency band of 12–48 s (hereafter referred to as Pi1-2 for brevity). These waves made their first appearance at the RABB (Rabbit Lake) station (see Figure 7.2), which enjoys a central location in the CARISMA magnetometer chain [*Mann et al.*, 2008]. The DWT analysis naturally provides appropriate timing uncertainties for each waveband, dependent on period. The timing uncertainty for the Pi1-2 is +/−20 s, demonstrating that the shorter period Pi1-2 waves provide the much-needed reduction in timing uncertainty for ionospheric observations in the auroral zone, namely well below the two-minute window that has previously impaired substorm research [*Ohtani*, 2004]. Figure 7.3 displays the onset times for Pi1-2 waves derived from a number of stations (triangles) as a series of timing contours that expand from the initial onset point (near RABB station). The arrival (or growth) of ULF waves in the ionosphere occurs at a clearly defined epicentre, and the later

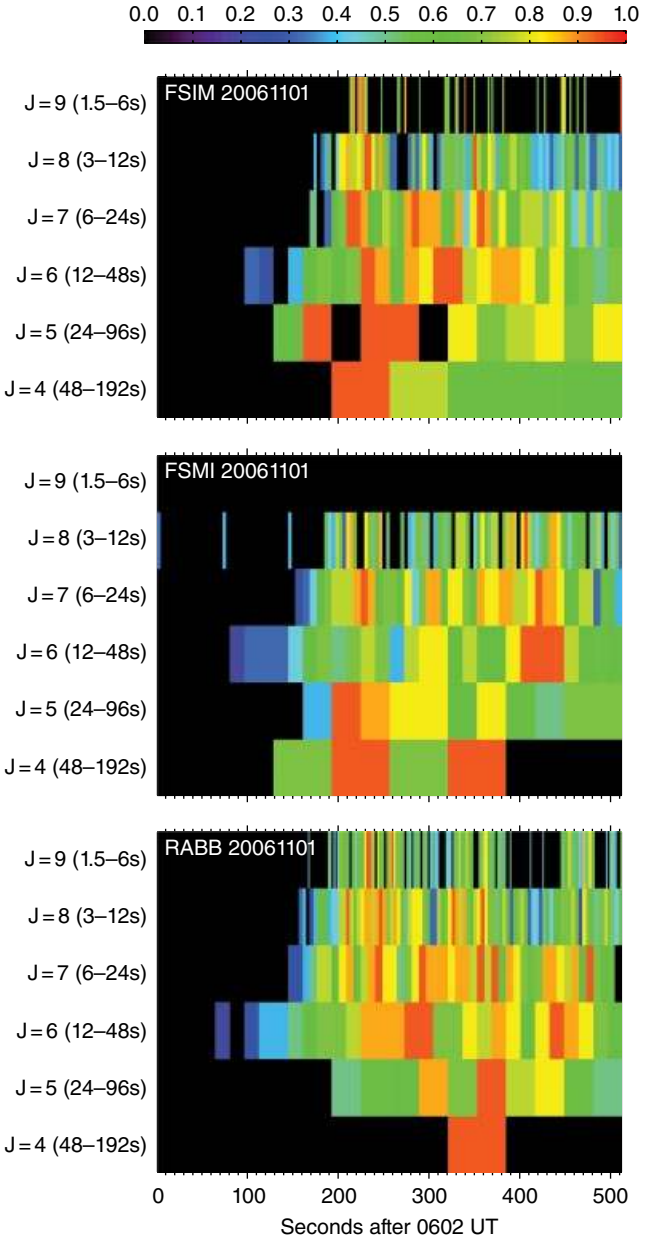

Figure 7.2 Discrete wavelet transform (DWT) of three ground magnetometers at the same latitude during the event (taken from *Milling et al.* [2008]).

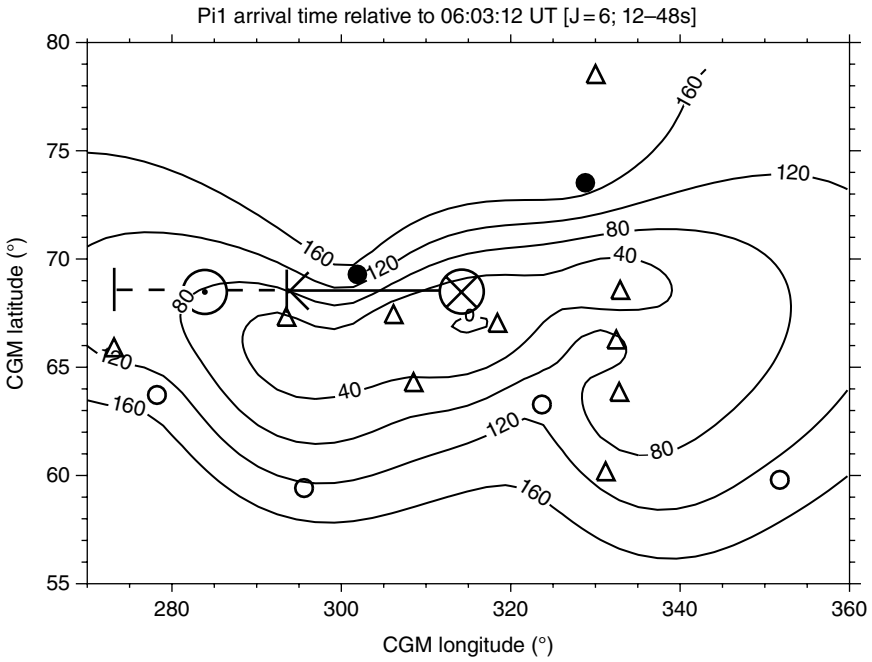

Figure 7.3 Arrival time of Pi1-2 ULF waves during an isolated substorm. Contours represent a spherical harmonic fit to the arrival times observed across the CARISMA and THEMIS magnetometer arrays, and the arrows represent the large-scale current of the SCW. Taken from *Milling et al.* [2008].

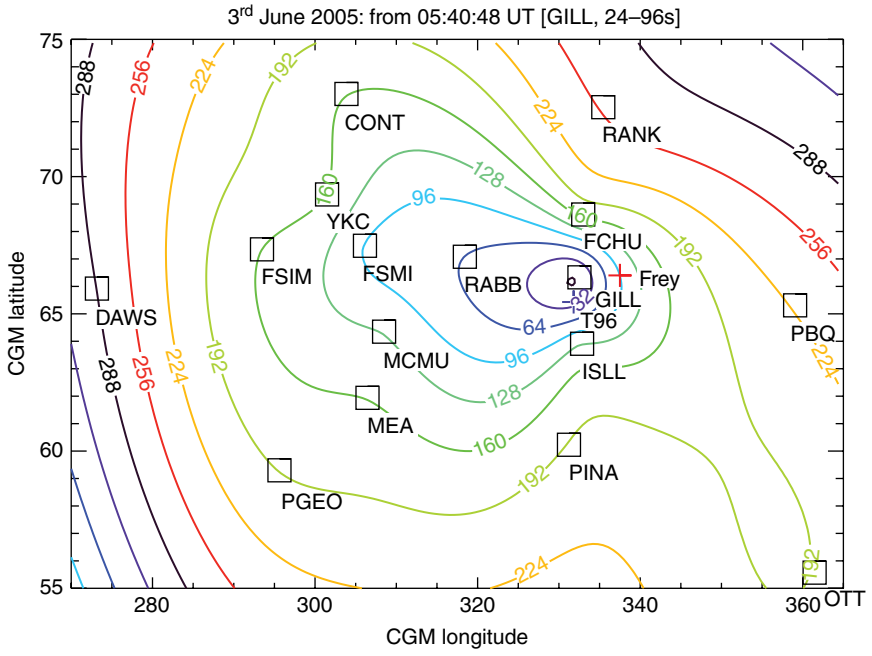

Figure 7.4 Arrival time of Pi1-2 ULF waves as in Figure 7.3 from *Murphy et al.* [2009], but as compared to the location of auroral brightening observed by the IMAGE FUV instrument from the Frey substorm list [*Frey and Mende,* 2007].

arrival (or growth) of ULF waves at other stations proceeds in an ordered fashion from the initial epicentre.

With the initial success of this technique, *Murphy et al.* [2009a] set about developing a more automated method to provide estimates of the onset of ULF waves in the ionosphere during substorms. The Automated Wavelet Estimation of Substorm Onset and Magnetic Events (AWESOME) technique designed by *Murphy et al.* [2009a] built upon the *Milling et al.* [2008] technique. A key part of the algorithm is use of an interactive adaptive threshold to determine the time at which ULF wave power rises above the preexisting noise, based on real

measurements (i.e., where the preexisting noise threshold is calculated by determining the ULF wave power prior to the substorm onset studied). The threshold algorithm provides a 98% confidence level that wavelet power coefficients above these thresholds are statistically significant and are not background noise. The onset time is robustly defined as the centre time of the first wavelet coefficient to exceed the threshold with an uncertainty of plus or minus the temporal width of the coefficient band.

To test the AWESOME algorithm, *Murphy et al.* [2009a] compared ULF wave onset times with the times of auroral intensifications as determined in the Frey substorm onset list [*Frey et al*., 2005; *Frey and Mende*, 2007]. Four case studies were identified where there were sufficient auroral and magnetic measurements to be compared directly with each other. Figure 7.4 shows one of these case studies, where the contours display the onset of ULF waves in the 24–96 s period band across the CARISMA and THEMIS ground magnetometers, at 32 s intervals. The *Milling et al.* [2008] result is demonstrated to be a repeatable phenomenon; there is also an epicentre to ULF wave activity in this substorm. Superimposed on these contours is the location of the substorm brightening as determined by *Frey et al.* [2005], in precisely the epicentre of the ULF wave contours. Interestingly, the ULF wave signature at the centre occurred several minutes prior to the times listed in the Frey database. This is perhaps not surprising for a number of reasons, but primarily because the IMAGE global auroral imager had a ~2 min cadence, and global auroral imaging responds primarily to a large-scale auroral breakup as opposed to the localized initial brightening of the substorm onset arc that defines auroral substorm onset. These studies have demonstrated the difficulties inherent in timing different substorm phenomena, and the "onset" of auroral brightening is naturally difficult to pinpoint [*Liou and Zhang*, 2009; *Murphy et al.*, 2009b]. Nevertheless, the AWESOME algorithm was successfully shown to provide robust and reliable ULF wave onset times and to verify that ULF waves occur at the same place as auroral substorm onset.

7.4. ULF WAVE EVOLUTION AND CHARACTERISTICS AT ONSET

One of the most important characteristics of substorm-related ULF waves is that their amplitudes increase exponentially with time through substorm onset. Figure 7.5 (left) shows H- and D-component magnetometer data from the onset station of the same substorm studied by *Milling et al.* [2008] in three different frequency bands from Pi1 to Pi2 frequencies. Figure 7.5 (centre) shows the amplitude envelope of the waves [e.g., *Kepko and McPherron*, 2001], which better displays the wave growth. However, even more accurate information on time evolution of the ULF wave power can be gleaned simply by plotting the amplitude data on a logarithmic scale (right), where clear signs of exponential growth are seen between 06:02:30 and 06:05:30 UT. The preexisting noise levels, the start and end times for exponential growth, as well as the growth rate of the waves can all be estimated and quantified with much greater confidence through the simple expedient of changing the *y*-axis.

Rae et al. [2011] performed a statistical analysis of the evolution of ULF wave power as a function of time using an independently verified list of auroral intensifications identified through visual inspection [*Nishimura et al.*, 2010]. ULF wave amplitudes were computed during each of the 256 events (Figure 7.6a), and a superposed epoch analysis of the wave amplitude relative to each auroral brightening time was performed. Each horizontal colored bar in Figure 7.6a shows the ULF wave amplitude during an auroral brightening event. In Figure 7.6b the superposition of ULF wave power shows that, in general, ULF wave power increases exponentially through auroral onset by an order of magnitude at the magnetometer station closest to the THEMIS ASI that observes the rapid auroral brightening. Not only do wave amplitudes grow exponentially during a time interval that encompasses onset, but the wave amplitudes remain elevated for at least 15 min after the expansion phase onset. ULF wave power and auroral brightness are inextricably tied together during periods of rapid increases in auroral intensity.

Murphy et al. [2011] performed a statistical analysis of the two-dimensional structure of ULF wave power across all Pi1–Pi2 ULF wave frequencies to identify the spatial characteristics of each ULF wave band during the interval surrounding substorm onset. An initial driver of this study was to investigate whether there were any statistical differences between the properties of waves within the traditional ULF frequency bands, or whether the boundaries between frequency bands are arbitrary in the context of substorms. *Murphy et al.* [2011] established that ULF wave power is concentrated near the location of substorm onset and that, statistically over many substorms, no wave frequency band dominates. Both Pi1-2 and Pi2 ULF waves display the requisite polarization characteristics as expected from the historical literature. All waves showed azimuthal angles that point toward the centre, upward, and downward FAC elements as per *Lester et al.* [1983] and *Gelpi et al.* [1987]. In addition, the ellipticity of the wave polarizations across all ULF wave bands varies, according to *Samson et al.* [1971], as a function of local time and latitude. Figure 7.7 shows the angle of azimuth for ULF waves within three overlapping frequency bands spanning 10–150 s periods. The expected rotation detailed by *Lester et al.* [1983], where the angle of azimuth is positive in the east, passes through zero to be negative in the west, is observed in all ULF wave bands.

In this section, we have established that the careful analysis of ULF waves measured by ground-based magnetometers in the auroral zone during the onset of the

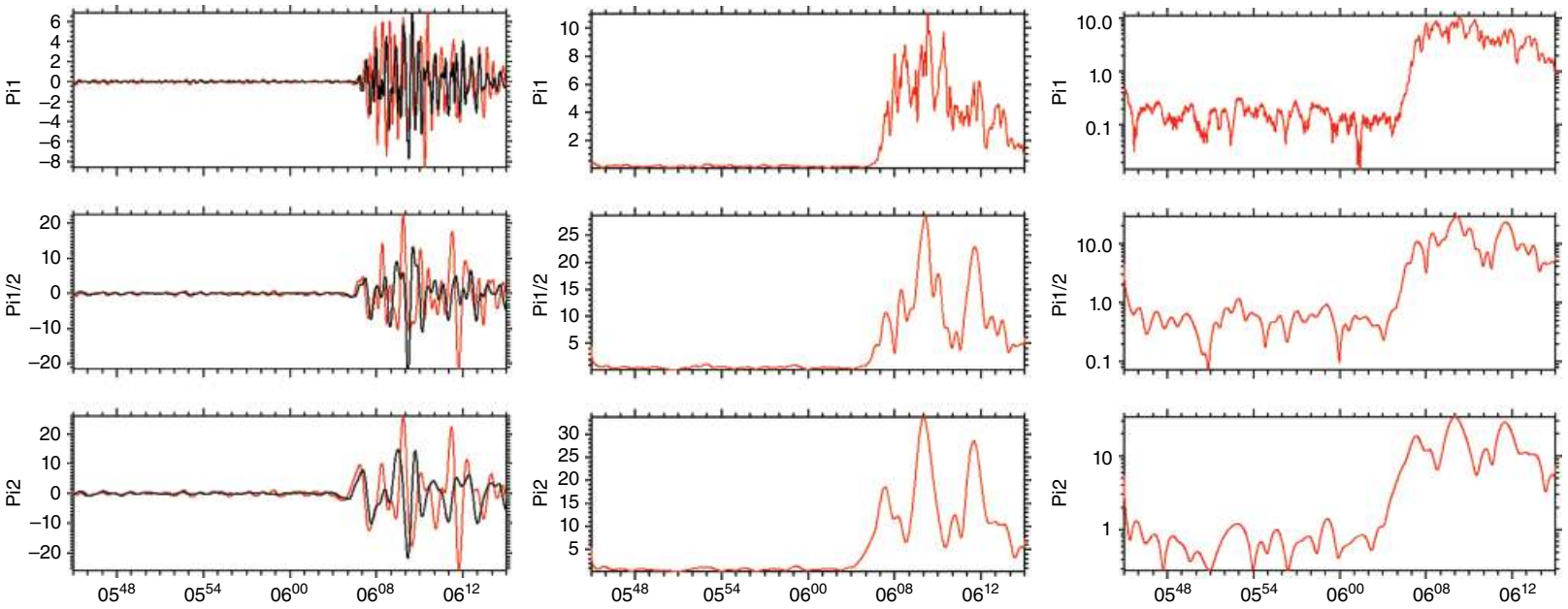

Figure 7.5 ULF waves in three different frequency bands from the onset station in the epicentre presented in *Milling et al.* [2008]. (left) Filtered H (red) and D (black) magnetometer data, (centre) the amplitude envelope of the ULF pulsations, and (right) the log of the amplitude envelope to demonstrate the utility of viewing ULF wave amplitudes on a logarithmic scale.

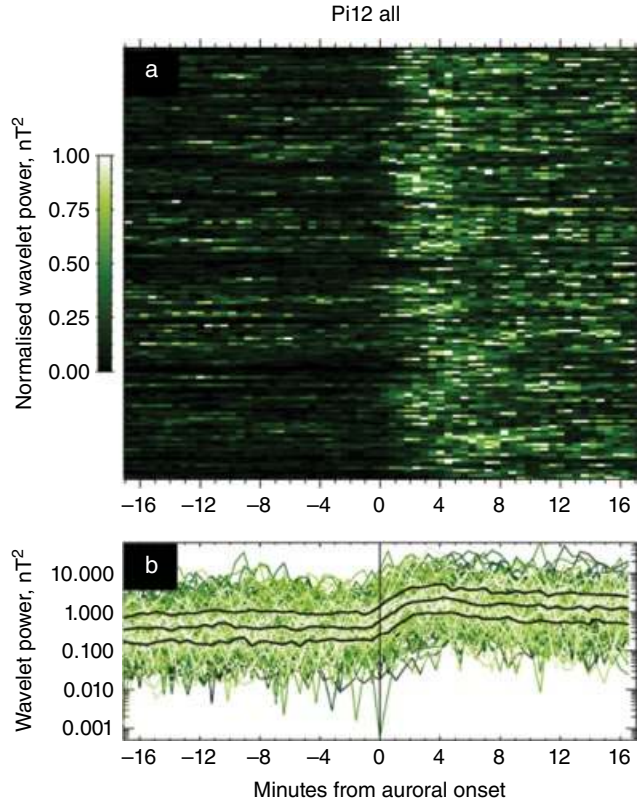

Figure 7.6 Statistical analysis of ULF wave amplitudes through substorm onset using a superposed epoch analysis of 256 substorms from *Rae et al.* [2011]. ULF wave amplitudes were studied from the ground-based magnetometer closest to the auroral expansion phase onset as identified by independent lists of substorm onset times. (a) Each horizontal line shows one case study magnetometer at the magnetometer closest to the onset location identified by *Nishimura et al.* [2010] and there are 256 lines being in the vertical direction, color represents normalized wave powers. (b) A superposed epoch analysis to demonstrate the general characteristics of Pi1-2 waves.

expansion phase can diagnose a number of important physical aspects of the substorm:

- Substorm ULF waves have a distinct epicentre that is co-located with the initial brightening of the onset arc and linked to the auroral location of the substorm current wedge;
- ULF waves during substorms demonstrate exponential growth;
- The time at which ULF waves across a broad range of frequencies (~10–100 s period) increases above the background noise at a particular station coincides with the time at which the aurora starts to brighten, as determined independently from auroral data;
- The polarisation characteristics of ULF waves across a broad range of frequencies (~10–100 s period) are similar and reveal the location and characteristics of the substorm current wedge.

7.5. AURORAL BEADS, AZIMUTHAL AURORAL FLUCTUATIONS, AND THE SUBSTORM

The first indication of a substorm is a "sudden brightening of one of the quiet arcs lying in the midnight sector of the oval (or a sudden formation of an arc)"; *Akasofu* [1977]). A detailed analysis of the sudden brightening of the auroral arc has demonstrated that during some events, the auroral brightening displays longitudinal structure and temporal variations that have ULF wave characteristics. In this section, we focus on the properties of ULF waves that are seen in two-dimensional images of auroral intensity near substorm expansion phase onset.

With the launch of the Swedish Viking mission in 1986, real-time monitoring of the auroral oval was available over an extended period of time, allowing new insight into the global auroral morphology during substorms. Viking had what was, at the time, cutting-edge spatial

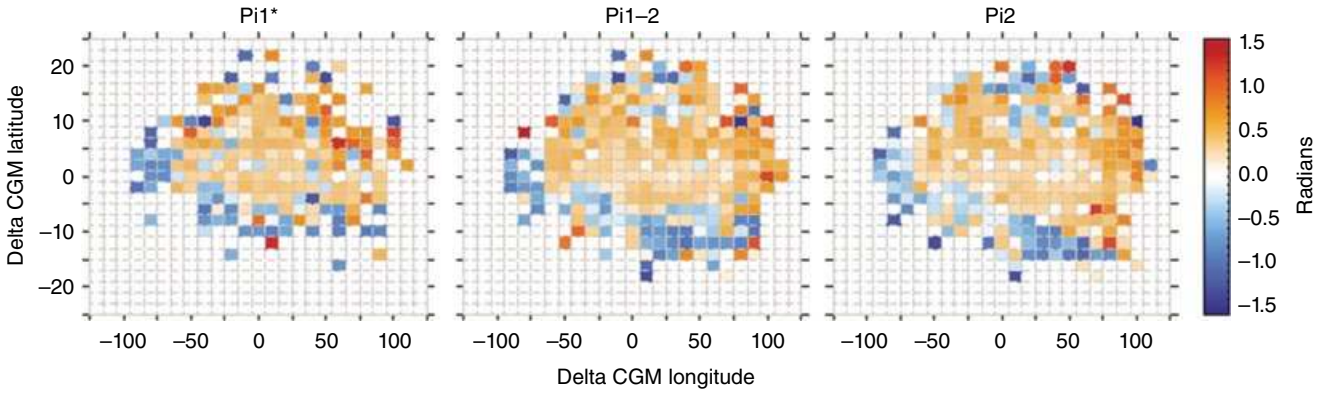

Figure 7.7 Median two-dimensional distribution of the ULF wave angle of azimuth with respect to auroral onset in the (left) Pi1*, (middle) Pi1–2, and (right) Pi2 wave bands. The color bar depicts the angle of azimuth in radians bounded by $[-\pi/2, \pi/2]$.

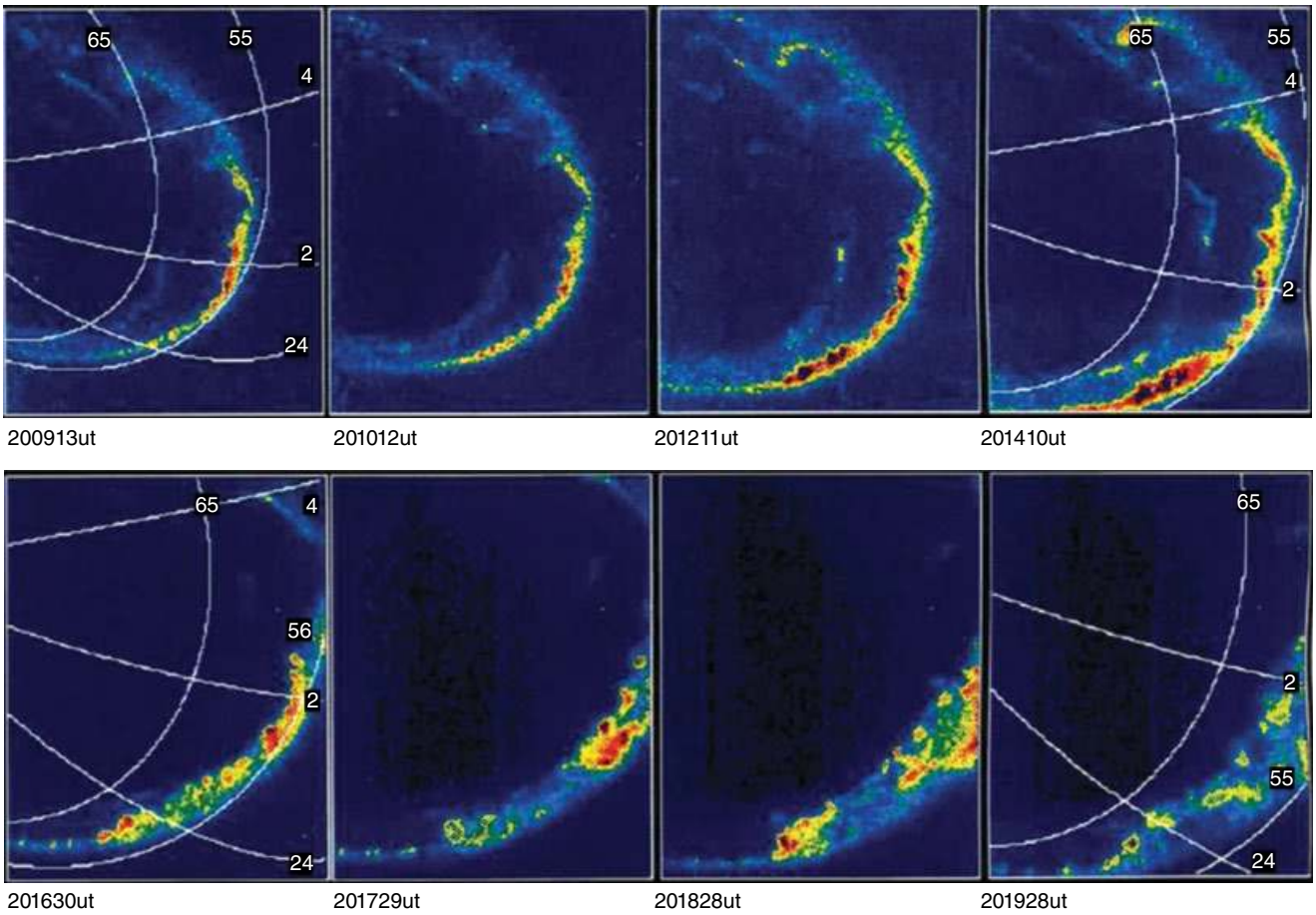

Figure 7.8 Auroral measurements from the UVI experiement [*Cogger et al.,* 1991] on the Viking satellite through an auroral substorm onset. Notable in the earlier frames are the existence of auroral beads, or azimuthal auroral forms as *Elphinstone et al.* [1995] subsequently called them. Reproduced from Figure 9.16, Henderson [1994].

resolution of 0.076° × 0.076° with <2 min temporal cadence [*Anger et al.*, 1987]. Figure 7.8 shows the first published mention of azimuthal auroral fluctuations immediately prior to a substorm auroral breakup, or "hot spots" and "spirals," as referred to by *Henderson* [1994]. These wave-like auroral fluctuations (first seen in the top left panel) occur on the equatorward branch of the auroral oval, deep inside the closed field line region, and as we move forward in time from one image to the next, the fluctuations grow in intensity and expand to larger scales in the region that subsequently breaks up closer to dusk.

Henderson [1994] postulated that it was difficult to identify what process or processes were responsible for this, although already the evidence suggested the action of a plasma instability. He writes: "the main problem in trying to assess [the possibility of the role of ballooning in onset] is that it is entirely unclear what a "ballooning substorm" should look like in the aurora." *Henderson* [1994] concluded that, since ballooning [e.g., *Roux et al.*, 1985, 1991] occurred in the region between dipole-like and tail-like field lines [e.g., *Samson et al.*, 1992], then ballooning was consistent with the formation and evolution of these auroral hot spots. Following *Henderson* [1994], *Elphinstone et al.* [1995] document the formation and evolution of azimuthally spaced auroral forms that occurred in the initiation phase of the substorm. Figure 7.9 shows a sequence of auroral images from the Viking satellite mission through a substorm on 24 November 1986 around 2000 UT. In the top row of Figure 7.9, the "double oval" configuration is evident. The poleward branch remains relatively undisturbed while the equatorward branch develops periodic longitudinal auroral structuring. These authors termed the equatorward structure "Azimuthal Auroral Forms", or AAFs. A series of AAFs begin around 20:05:15 UT, and grow in amplitude between this initial time and the poleward expansion and (in this case) westward expansion of the subsequent auroral bulge. Note that without information regarding the auroral intensity scale in this study, we are unable to investigate the nature of the increase in auroral intensity during this event. *Elphinstone et al.* [1995] found that in 26 of the 37 events studied, AAFs did indeed precede the substorm onset,

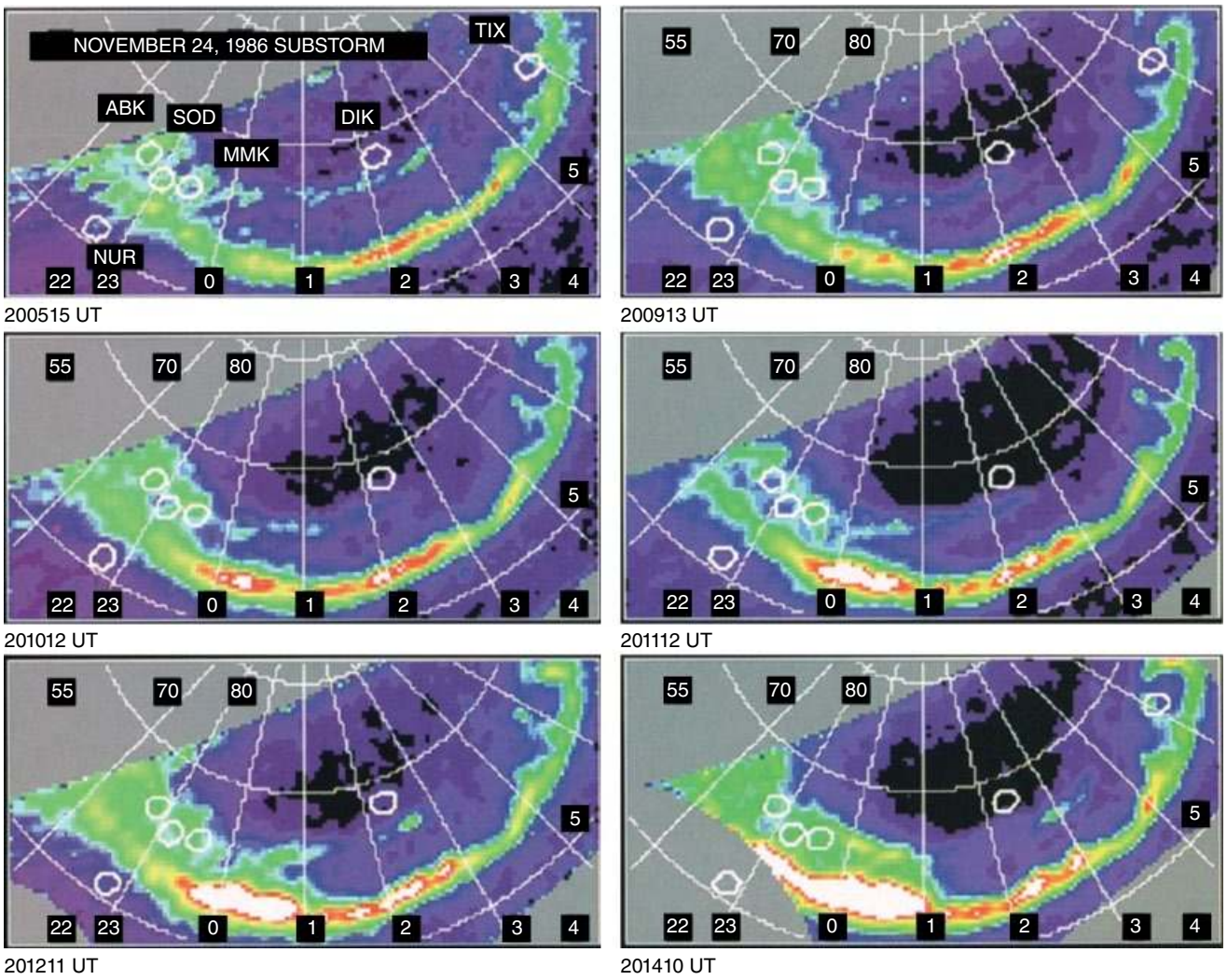

Figure 7.9 Observations of an auroral substorm via a sequence of auroral images from the Viking satellite mission in magnetic latitude and magnetic local time coordinates, with their values labeled accordingly. From *Elphinstone et al.* [1995], Plate 2.

and they demonstrated that their spatial wavelengths span the range 132–583 km, with an average wavelength of 307 ± 115 km (see Figure 7.10).

Although these results tell us much about the spatial structure of auroral forms during substorm expansion phase onset, there are two important caveats:

• The lower wavelength cutoff is stated not to be instrumental artefact due to pixel size. *Elphinstone et al.* [1995] state that the minimum pixel size from Viking should be able to resolve wavelengths of less than the cutoff of 130 km, and so the cutoff is either physical, or a sensitivity issue.

• It is difficult, if not impossible, to understand the formation, evolution, and relevance of auroral features relative to substorm onset with observations that have a ~2 minute cadence.

Surprisingly, there have been few further reports of azimuthally spaced auroral fluctuations from space-based

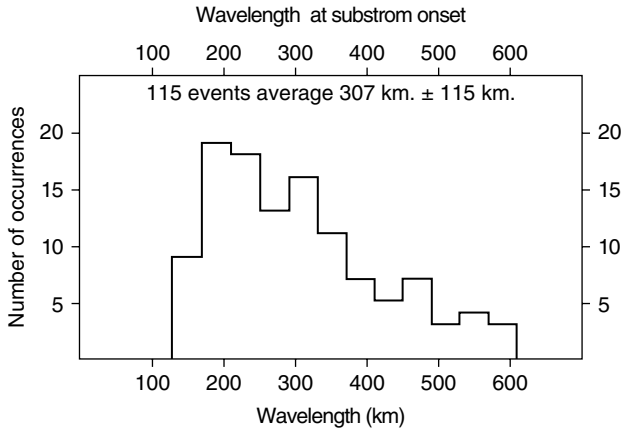

Figure 7.10 Occurrence rate of the spatial scales associated with AAFs prior to substorm onset. Note that this statistical study comprised 27 substorm onsets and 115 measurements within these substorm onsets, and so temporal evolution is implicitly included in this figure. From *Elphinstone et al.* [1995], Figure 8.

measurements. Using the FUV/WIC auroral imager onboard the IMAGE satellite, *Henderson* [2009] presented a substorm on 21 November 2002 that also displayed longitudinal auroral structuring in advance of substorm onset. Figure 7.11 shows a summary of the results, showing spatial evolution of the AAFs as a function of time during this event. *Henderson* [2009] did not calculate an azimuthal wavelength for this interval but did calculate

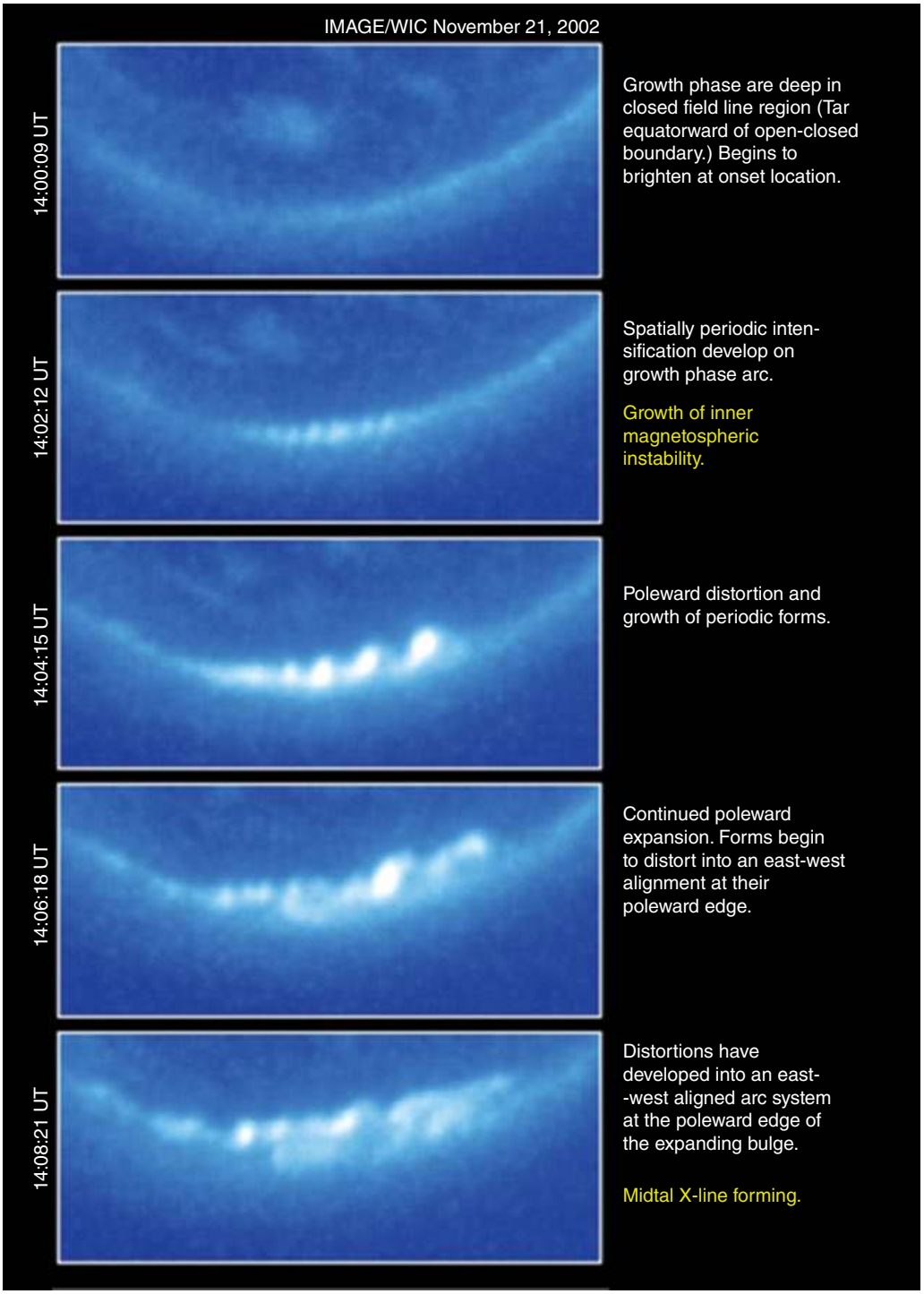

Figure 7.11 Evolution of the most equatorward arc system as a function of time through substorm onset. The first visible signs of auroral structuring appear in the 14:02:12 UT image, which evolve into lower azimuthal wavelengths that brighten as a function of time. From *Henderson* [2009], Figure 2.

the time for exponential growth, or growth rate, to be 188 s, or 0.0053/s, again associating these observations with a ballooning instability on closed field lines close to the Earth. As *Henderson* [2009] notes, "such spatially periodic auroral spots have been seen prior to the onset of substorm expansion phase in other studies as well (*Henderson*, 1994; *Elphinstone et al*., 1995; *Samson et al.*, 1996; *Voronkov et al*., 2000, 2003)." Although not all of these papers directly discuss substorms, in particular the *Samson et al.* [1996] and *Voronkov et al.* [2000, 2003] papers would, with what we know now, be clearly linked to substorms. Later in this chapter, we will study a wider range of magnetotail instabilities that could be responsible for the azimuthally structured auroral forms at substorm onset.

7.6. AZIMUTHAL AURORAL FORMS AS MEASURED BY THE THEMIS ASIS

In auroral physics, some compromise exists between large-scale measurements from global auroral imaging (e.g., Polar, IMAGE) that provide long periods of entire hemispheric coverage at ~100 km spatial resolution at low (~30–120 s) cadence, localized *in situ* measurements of auroral measurements from LEO satellites (e.g., REIMEI) that rapidly pass over regions of interests, and ground-measured high cadence and local fast auroral imaging [e.g., *Trondsen et al.*, 1997; *Knudsen et al.*, 2001; *Semeter et al.*, 2005; *Partamies et al.*, 2010] that provide only local observations of the aurora. The advent of the ground-based component of the NASA THEMIS mission presented an unique opportunity to probe the aurora across unprecedented spatial and temporal scales. With these ground-based measurements comprised of 21 auroral imagers that formed an overlapping array, it was possible to probe the occurrence and evolution of auroral beads at ~1s resolution, 1 km spatial scales and across 8 to 12 hours of local time. As a consequence of this increased coverage and cadence, several authors began to rediscover the small-scale structuring along some substorm onset arcs and link these to substorm onsets as *Henderson* [1994] and *Elphinstone et al.* [1995] did. The contributions in this regard include *Donovan et al.* [2007, 2008], *Liang et al.* [2008], *Sakaguchi et al.* [2009], and *Rae et al.* [2009a, 2009b], all of which present evidence of small-scale arc beading during the initiation of substorms and pseudo-breakups. More quantitatively, *Sakaguchi et al.* [2009], and *Rae et al.* [2009a, b] provide estimates of azimuthal wave numbers, m, with values >100, and have also demonstrated that the auroral beads precede observed signatures of magnetic reconnection (e.g., *Murphy et al.*, 2015).

Earlier in this chapter, we demonstrated that the ULF wave epicentre occurs at the same location of auroral breakup, but minutes prior to auroral breakup [*Murphy et al.*, 2009a, b]. Seeking to understand the nature of this ULF wave epicentre, *Rae et al.* [2009a, b] used the AWESOME magnetic field time-series technique to study several substorms during the THEMIS era, where detailed mesoscale auroral observations could be made routinely at ~1 km spatial scales using the THEMIS ASI. The ULF wave epicentre was discovered to occur both in the same location and at the same time as the first indication of auroral brightening along the substorm arc. The auroral fluctuations along the arc, first termed "auroral beads or hot spots" by *Henderson* [1994], "azimuthal auroral forms" by *Elphinstone et al.* [1995] have subsequently been re-christened "auroral beads" in recent history. Since these terms are interchangeable in the literature, we revert to the original *Henderson* [1994] description of auroral beading.

Interestingly, although the ULF wave epicentre is intimately associated with auroral beads, substorm activation during periods of extended activity can be more complicated. *Rae et al.* [2009a] studied a substorm onset that occurred after multiple beaded auroral activations and found that the onset of each interval of beading coincided with an individual magnetic ULF wave epicentre. Only after the final auroral activation was the substorm initiated (see Figure 7.12). While north–south auroral forms were also observed during this event, neither auroral streamers (e.g., *Nishimura et al.*, 2010) nor auroral beading appeared to be sufficient to produce a traditional substorm auroral breakup during the first few activations.

Auroral beads and the ULF wave epicentre occur at the same time and the same place, but do they have the same frequency characteristics? Again, the rapid temporal cadence of the THEMIS ASI array has proved invaluable. At the beginning of an isolated substorm within the THEMIS ASI fields of view during an event in the centre of the ground-based magnetometer network in Canada, *Rae et al.* [2009b] showed that the frequency of the auroral beading was in exactly the same frequency band as the first magnetic ULF waves to be observed. In this case, the frequency band was the long period Pi1–short period Pi2, or 24–96 s period band (Pi1-2 discussed earlier). For this isolated substorm, there is also a ULF magnetospheric signature in the same frequency band at geosynchronous orbit. Increasingly, it seems that a plasma instability in the near-Earth plasmasheet is most likely responsible for the detonation of this substorm (Figure 7.13).

We know from the ground-based magnetometer observations that ULF wave power increases exponentially by about an order of magnitude during rapid auroral brightenings [*Rae et al.*, 2009]. It is well known that auroral intensities start to increase exponentially at substorm onset [e.g., *Henderson*, 2009], and so logically to understand the linkage between ULF wave signatures observed in auroral and magnetic data, it is necessary to study the temporal evolution of both. The characteristics of exponential growth of optical and magnetic ULF wave

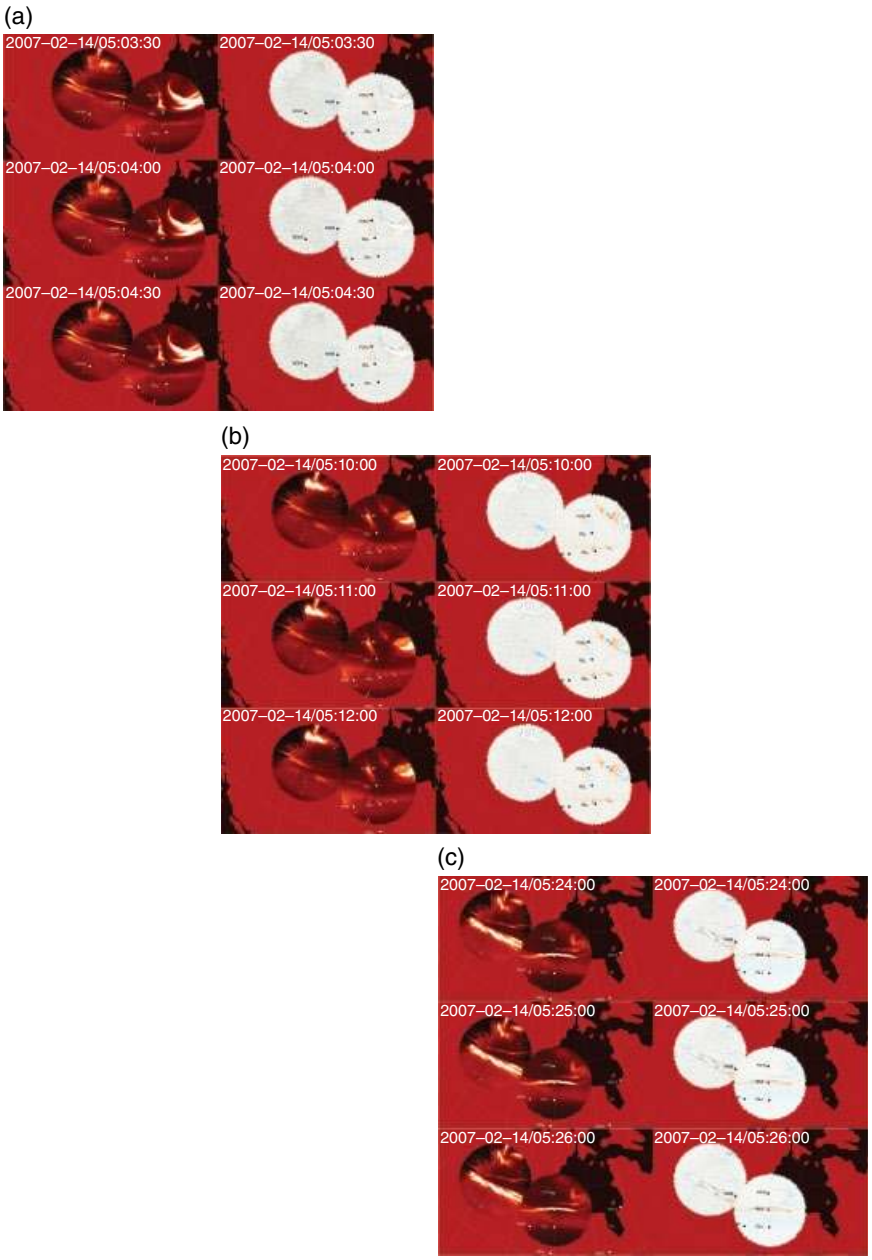

Figure 7.12 In each panel, to the left are the false color images and to the right the 3 s difference images from the FSMI and GILL ASIs for the three consecutive auroral bead onsets at: (a) ~0503 UT, (b) ~0510 UT, and (c) ~0524 UT. On 14 February 2007.

signatures during the substorm are shown in Figure 7.14 [*Rae et al.*, 2012], demonstrating that not only do the waves occur at the same time, the same place, and with the same frequencies, but both the auroral intensity and ULF wave power grow exponentially over the same number of orders of magnitude and at roughly the same rate. From the ionospheric measurements, we reach the inescapable conclusion that the ULF wave signatures in the magnetic field and in the aurora are caused by the same magnetospheric instability phenomenon.

Others, however, disagree. Studying the two-step evolution of Auroral Kilometric Radiation (AKR), *Morioka et al.* [2014] present analysis of conjugate ground magnetometer data to their AKR signatures. *Morioka et al.* hypothesized that the increase in ULF wave amplitudes at auroral latitudes during expansion phase onset may

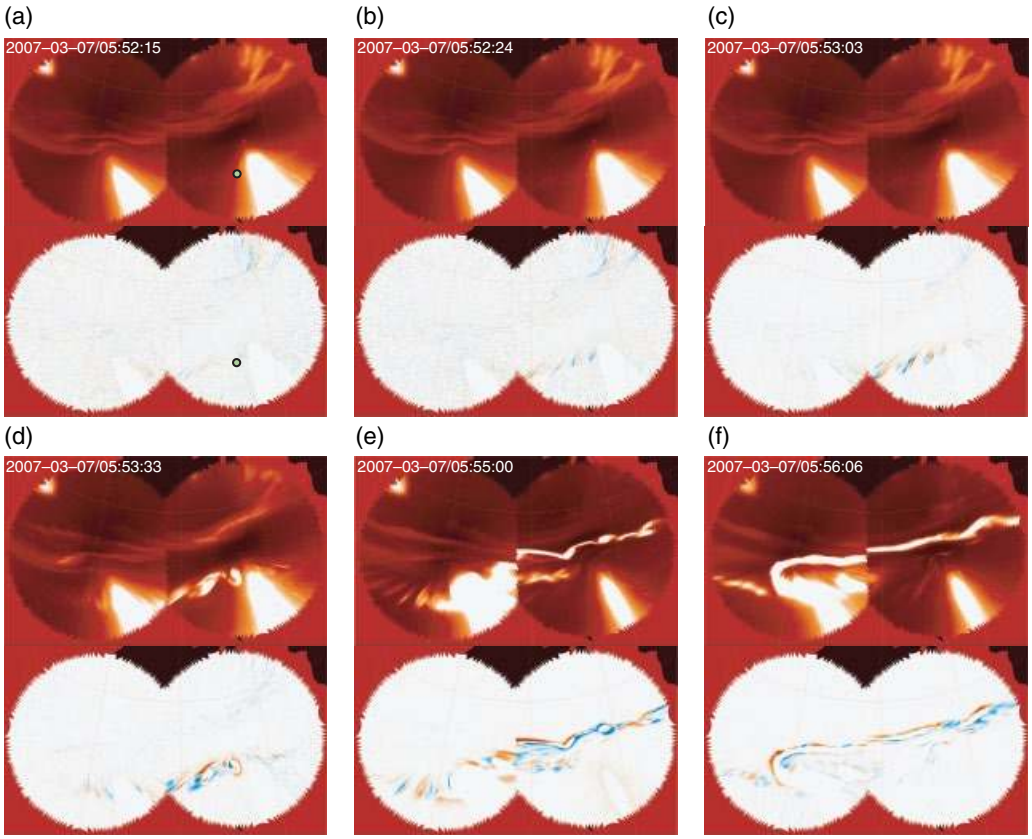

Figure 7.13 A time sequence (a–f) through a substorm onset. In each panel (a–f), the top image shows a false color image of white light intensity and the lower image is a false color representation of the difference between the current ASI images and the image from the prior 3 s. The bright region in the top panel, bottom right, shows the signature of the moon (not removed to maintain the integrity of the image). In the bottom panels, red represents the appearance of new emissions, blue the disappearance of prior emissions, and the lunar signature is therefore removed. For context, the green/black dot in the first panel in the SNKQ FOV shows the T96 [*Tsyganenko,* 1995] tracing of the ground magnetic footprint of GOES-12. An auroral bead driven substorm on 7 March 2007. Taken from *Rae et al*. [2009a].

instead be related to new acceleration regions developing at high altitudes in the magnetosphere-ionosphere coupling region, not the inner plasma sheet. From this, *Morioka et al.* [2014] conclude that the magnetic Pi2 waves (40–50 s period) observed are likely a signature of a magnetospheric instability, whereas the Pi1 waves (10–30 s period) are a signature of intensified FACs in conjugate M-I coupling regions. Although *Morioka et al.* [2014] provide compelling evidence that the AKR generation during substorms is a two-step process, it is necessary to question the ULF data more deeply. Briefly, Figure 8 of *Morioka et al.* [2014] shows three limited frequency ranges derived from fluxgate measurements, but analyzed as a variometer using dH/dt as opposed to $H(t)$, effectively forming a poor high-pass filtering of the data. As seen in Figure 7.2 and Figure 7.5, ULF wave onset across all frequencies occur within 10 s, and the waves can only be seen to grow exponentially out of the magnetic noise on a logarithmic scale or by quantitative analysis through tools such as AWESOME or Hilbert–Huang transform. This means that low-amplitude high-frequency ULF waves cannot be visually identified without analysis at least on a logarithmic scale. One interesting aspect, however, is the assertion by *Morioka et al.* [2014] that 40–50 s period ULF waves are the signature of a magnetotail instability, which is entirely consistent with the results presented in this chapter. Moreover, we do not limit ourselves to a narrow frequency band; we use instead a broader frequency range that overlaps both the long-period Pi1 and short-period Pi2 bands, since there is no physical distinction between ULF waves of 30 s and 50 s periods, other than the artificial boundary at 40 s initially identified by *Jacobs et al.* [1964] as a matter of practicality.

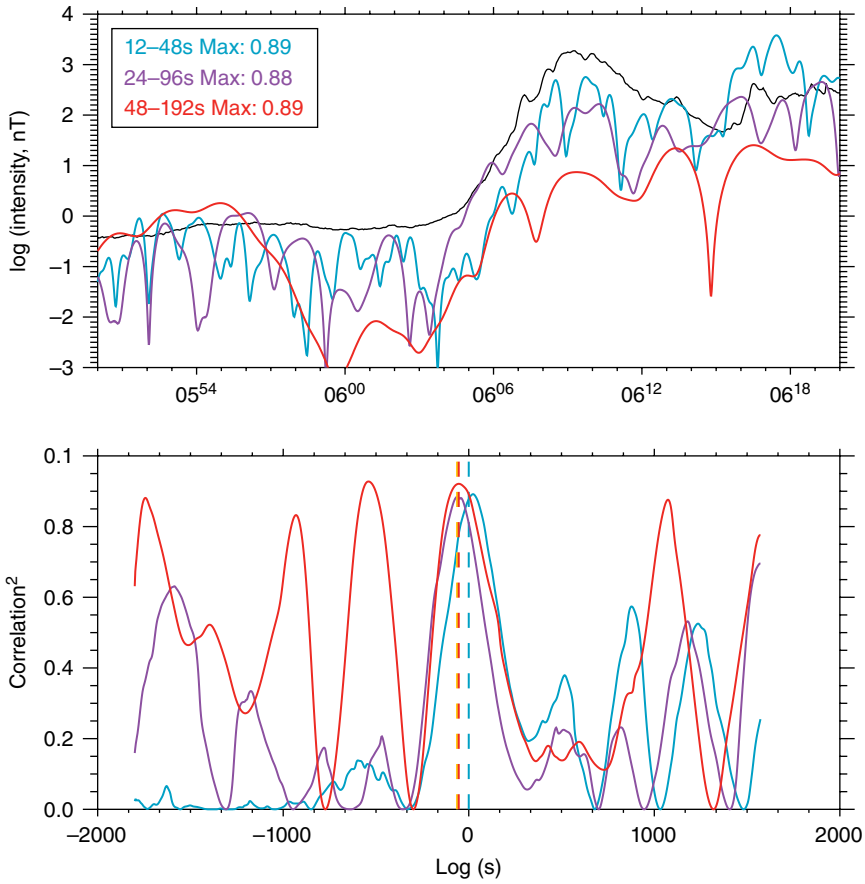

Figure 7.14 (top) Wavelet-filtered ground magnetic amplitudes in the 6–24, 12–48, 24–96, and 48–192 s ULF wave bands, together with the ASI intensity shown in Figure 7.2 (top left). (bottom) Correlation coefficients of the amplitudes of each of the wavelet period bands with the ASI intensity as a function of relative lag during the period of exponential growth, 0600–0610 UT. Adapted from *Rae et al.* [2011].

Whether or not specific ULF wave modes are physically linked to different source regions, there is a multitude of publications devoted to discussions on intermediate processes between the magnetosphere and ionosphere that may be involved in the structuring or otherwise of field-aligned currents associated with substorm aurorae. Structuring of these mechanisms include, but are not limited to, ionospheric feedback instability [*Lysak*, 1991], Ionospheric Alfvén Resonator [*Lysak and Song*, 2008], Kelvin–Helmholtz or tearing instabilities [e.g., *Chaston and Seki*, 2010], to name but a few. For a review, see *Dahlgren et al*. [2015]

Here, we investigate the simplest explanation of the exponentially growing ULF wave power observed in auroral displays and ground-based magnetometers: that a magnetospheric instability in the inner plasma sheet generates ULF waves that propagate from the plasma sheet to the ionosphere in the form of shear Alfvén waves [e.g. *Wygant et al.*, 2000], accelerating electrons to provide the aurora [*Watt and Rankin*, 2009, 2010, 2012]. Additionally, we will explore the different types of magnetotail instabilities that may occur at the inner edge of the plasma sheet, since there is evidence that substorm onset aurora is associated with acceleration by shear Alfvén waves [*Mende et al.*, 2003].

The first attempt to identify conjugate correlative ULF wave growth in space was made by *Walsh et al.* [2010]. In this study, Double Star was magnetically conjugate to signatures of exponential ULF wave growth on the ground. However, a small but critical ~10 s data gap at precisely the wrong time frustrated attempts to relate the electromagnetic wave and electron signatures in space to those measured on the ground.

To summarize, there is a startling interrelationship between optical and magnetic signatures of substorm onset:

- A magnetic ULF wave epicentre occurs at the same location as auroral onset [*Murphy et al.*, 2009a, b];
- A magnetic ULF wave epicentre occurs as the same time and location as the formation of ULF wave auroral beading along the substorm onset arc [e.g., *Rae et al.*, 2009a, b];

• Magnetic ULF wave amplitudes and auroral intensities both grow exponentially during auroral substorm onset and are highly correlated in amplitude and time through substorm onset (Figure 7.14) [*Rae et al.*, 2012].

7.7. SPATIAL CHARACTERISTICS OF ULF WAVES AT SUBSTORM ONSET

Due to the integration effects of a magnetometer that responds to any and all currents flowing in the ionosphere, it is difficult to establish any detailed spatial information regarding the structure of the ULF waves from ground-based magnetometry alone. However, there is strong evidence that the magnetic ULF waves and the auroral fluctuations are ionospheric manifestations of the same phenomenon. The two-dimensional nature of the auroral images provides us with the means to study the spatial and temporal characteristics of individual ULF modes at substorm onset, so we will now look at these data more closely. Of specific interest is the fact that the temporal behavior of the optical and magnetic signatures occurs in the same period band; that is, the 24–96 s period corresponding to long-period Pi1/short period Pi2 frequency band discussed above.

The two-dimensional auroral images can be processed further in order to extract information regarding the growth rates as a function of spatial wavenumber [*Rae et al.*, 2010]. For each 3 s interval, the data are transformed into a corrected geomagnetic coordinate system referenced to 110 km altitude. Figure 7.15a shows the longitudinal variations of the aurora in a slice taken at a certain latitude and the temporal evolution of the auroral brightness as a function of longitude at 63.7° CGM latitude. The intensity of the auroral structures grows throughout the interval shown until around 05:53:30 UT. Each vertical section of Figure 7.15a is Fourier transformed in the spatial domain to give auroral intensity as a function of wavenumber, and then the evolution of each wave mode is studied in time. The evolution of the wave amplitudes is shown in Figure 7.15b. Almost all the wavenumbers $<1.5 \times 10^{-4}$ m^{-1} exhibit exponential growth. The growth rates for each wavenumber are calculated, and plotted in Figure 7.15c. Note that growth rates are peaked at low $k = 5 \times 10^{-5}$ m^{-1}, with values ~0.1 s^{-1}, which means that growth is largest at ~50 km and grows on timescales shorter than the period of the fluctuations.

7.8. WHAT PHYSICAL MECHANISMS FIT THE AZIMUTHAL STRUCTURING AND EXPONENTIAL GROWTH OF THE SUBSTORM ONSET ARC?

Although small-amplitude auroral fluctuations have been found to be present during both the growth phase and the expansion phase by *Uritsky et al.* [2009], these authors conclude that ULF waves are not involved in the onset process because they are observed continually during a long time interval encompassing the shorter period of substorm expansion phase. However, the exponential increase of the intensity of these fluctuations exactly at the substorm expansion phase means rather the opposite. Whether or not fluctuations are present for a long time prior to substorm onset, the exponential growth of the intensity of these structures across a range of spatial scales is a tell-tale hallmark of a linear plasma instability operating in space. Moreover, by looking at the rate of exponential growth (growth rate) as a function of azimuthal mode number (or k), we not only can conclude that an instability is operating but also can estimate which instability, remarkably from ground-based instrumentation alone. We explore this hypothesis below by detailing key physical aspects of potential instabilities and ruling these in or out as potential candidates depending on their growth rate, spatial scales, and wave frequencies.

Figure 7.15d shows the azimuthal and radial structuring deduced from the auroral imagers mapped out from 110 km altitude into the equatorial magnetosphere using a simple Tsyganenko 96 magnetic field model. In this event, the radial extent was estimated to be ~0.7 R_E and the azimuthal wavelength ~0.35 R_E at geosynchronous orbit, which of course is magnetic field model dependent. If we investigate different candidates for plasma instabilities at this location, then we require a few plasma parameters in order to study the predicted growth rates and growing wavenumbers. The equatorial magnetic field strength at this location is 90 nT (as measured at GOES), and hence the proton gyrofrequency $\Omega_i \sim 7$ rad s^{-1}. We also estimate a number density of $n_i \sim 10^6$ m^{-3} and an ion temperature of 10 keV in the equatorial plane based on the general plasma sheet characteristics around geosynchronous orbit in the magnetotail [e.g., *Wang et al.*, 2006]. We can now begin to identify which plasma instabilities can be ruled in or ruled out.

We can rule out a number of plasma instabilities that could be responsible for the growth and structuring of auroral beads because they do not fit the growth rate range or wave frequencies observed in the ionospheric auroral data [*Rae et al.*, 2010]. We then compare our growth rates and wave frequencies with published theoretical treatments or numerical simulations of each instability. Although from a magnetospheric platform, we would expect to observe a Doppler-shifted frequency in any observations of the instability, these simulations predict growth rates and frequencies that would be observed by a slowly moving satellite (or ground station), since the wave frequencies are calculated in the rest frame of the simulation. Table 7.2 outlines the candidate list of instabilities considered by *Rae et al.* [2010] to be able to explain their observational results, the frequencies and growth rates of the magnetospheric instabilities allowing *Rae et al.* [2010]

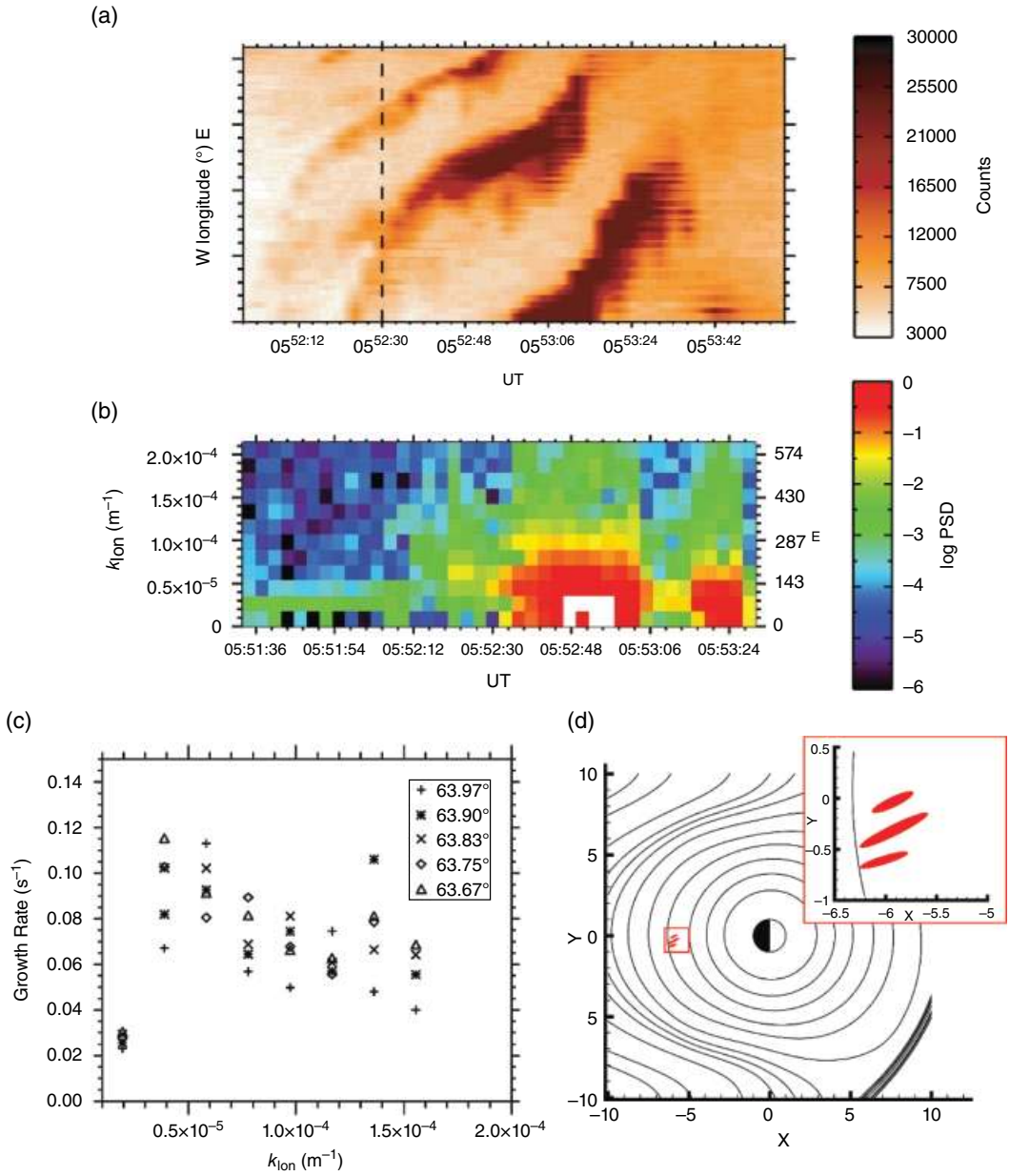

Figure 7.15 (a) Time series of east–west cuts through the THEMIS ASI data from the GILL station in a direction perpendicular to the breakup arc orientation. (b) Auroral fluctuations as a function of spatial wavelength (k_{lon}) and time. (c) Estimated growth rates γ as a function of k_{lon}. (d) Estimated source location of the auroral undulations in the equatorial plane ($Z_{GSM} = 0$) of the magnetosphere (red). Black lines indicate contours of constant magnetic field strength in the T96 magnetic field model. The inset shows an enlarged view of the region. Adapted from *Rae et al.* [2010].

Table 7.2 Potential instability mechanisms invoked to explain substorm onset, and whether their characteristics can explain the observational result of *Rae et al.* [2010].

Instability	Reference	Frequency	Growth Rate	Candidate?
Tearing	*Coppi et al.* [1966]	Possible	Too slow	No
Drift kink/sausage	*Zhu and Winglee* [1996]	Possible	Too slow	No
Current driven Alfvénic	*Perraut et al.* [2000]	Too high	Too high	No
Lower-hybrid drift	*Yoon et al.* [1994]	Too high	Too high	No
Kelvin–Helmholtz	*Yoon et al.* [1996]	Plasma dependent	Plasma dependent	Unknown
Entropy anti-diffusion	*Lee et al.* [1998]	Plasma dependent	Plasma dependent	Unknown
Cross-field current instability	*Lui et al.* [1991]	Possible	Possible	Yes
Shear-flow ballooning	*Voronkov et al.* [1997]	Possible	Possible	Yes
Kinetic ballooning	*Horton et al.* [2001]	Possible	Possible	Yes

to rule in or rule out each instability as the driver of auroral beads. Our analysis reveals that both the cross-field current instability [*Lui et al.*, 1991] and a form of ballooning, either shear flow [e.g., *Voronkov et al.*, 1997] or kinetic [e.g., *Horton et al.*, 2001; *Cheng*, 2004], possess identical growth rates and spatial scales to those estimated in studying the evolution of auroral beads. We note that some instabilities depend so heavily on plasma parameters that we cannot rule them in or out (e.g., Kelvin–Helmholtz instability). Our results suggest that the next important source of information on the detonation of the substorm will be from spacecraft that have traversed the nightside region of more dipolar field lines close to the Earth, which are necessary to reveal the nature of the plasma instability and the free energy that drives it.

7.9. CONCLUSION

In this review, we have demonstrated that a repeatable and robust signature of substorm onset is the formation of auroral *and* magnetic ULF waves, and that this signifies the start of the substorm at least in the ionosphere. This conclusion is only possible based on data from upgraded ground-based instrumentation networks. We have presented evidence that:

- the physical cause of the substorm onset arc *must* be related to ULF waves;
- the instability that drives the onset arc is highly peaked at low *k,*
  - shear-flow or kinetic ballooning,
  - cross-field current instability,
  - others that display this relationship depending on plasma parameters.

Determining the magnetic topology and plasma environment around the instability location(s) are key to solving this long-standing scientific problem. What remains is to discover which instability is responsible, and to find the source of the free energy that drives it.

ACKNOWLEDGMENTS

We are grateful to J. C. Samson for pestering us to start this work and for extended encouragement to continue along this path. We hope to finish this one day to his satisfaction. We thank M. G. Henderson for extended discussions regarding auroral hotspots. Now known as auroral beads, these phenomena were first discussed in his PhD thesis in 1994. We also thank K. R. Murphy, I. R. Mann, D. K. Milling, G. Rostoker, L. G. Ozeke, A. Kale, and K. Kabin for their significant input in creating this tremendous body of work. We would like to acknowledge active collaboration with the University of Alberta, Ian Mann and the CARISMA ground magnetometer group over the past decade (http://www.carisma.ca), without whom this work would not have been possible. CARISMA is operated by the University of Alberta, and funded by the Canadian Space Agency (CSA) in both the Canadian Geospace Monitoring, and now in the Geospace Observatory Canada, programs. We would like to acknowledge all of the NASA THEMIS mission team. In particular, we would like to thank V. Angelopoulos and H. Frey for their great help in this work under NASA Grant NAS5-02099 and NSF for support of GIMNAST through grant AGS-1004736. We also acknowledge S. Mende and E. Donovan for use of the THEMIS ASI data, the CSA for logistical support in fielding and data retrieval from the GBO stations.

IJR is funded in part by the UK Science and Technology Facilities Council (STFC) grant ST/L000563/1, and Natural and Environmental Research Council (NERC) grants NE/L007177/1 and NE/M00886X/1. CEJW is funded in part by the UK STFC grant ST/M000885/1.

REFERENCES

Akasofu, S.-I. (1964), *Planet Space Sci., 12*, 273–282.
Akasofu, S. I. (1977), *Quarterly Journal Royal Astronomical Society*, *18*, 170-187.
Akasofu, S.-I., and J. R. Kan (1982), *Planet. Space Sci., 30*, 1315.
Akasofu, S.-I. (2015), *Earth, Planets, Space* (submitted).
Angelopoulos, V. (2008), *Space Sci. Rev., 141*, 5–34.
Arnoldy, R. L., et al. (1987), *J. Geophys. Res., 92*, 12221.
Anger, C. D., et al. (1987) *J. Geophys. Res.*, *14*, 387–390.
Bosinger, T., et al. (1981), *J. Atmos. Terr. Phys., 43*, 933–945.
Bösinger, T., and A. G. Yahnin (1987), *Ann. Geophys, 5*, 231–238.
Bösinger, T. (1989), *Ann. Geophys., 7*, 375–386.
Coppi, B., et al. (1966), *Phys. Rev. Lett., 16*, 1207–.
Chaston, C. C., and K. Seki (2010), *J. Geophys. Res.*, *115*, A11221, doi:10.1029/2010JA015536.
Cheng, C. Z. (2004), *Space Sci. Rev.*, *113*, 207–270.
Dahlgren, H., et al. (2015), *Geophys. Res. Lett.*, *42*: 1290–1296, doi:10.1002/2015GL063173.
Elphinstone, R. D., et al. (1995), *J. Geophys. Res.*, *100*, 7937–7969.
Frey, H. U., et al. (2004), *J. Geophys. Res.*, *109*, A10304, doi:10.1029/2004JA010607
Frey, H. U., and S. B. Mende (2007), *Proc. Eighth International Conference on Substorms (ICS-8)* pp. 71–75.
Gelpi, C., et al. (1987), *J. Geophys. Res., 92*(A3), 2447–2460, doi:10.1029/JA092iA03p02447.
Heacock, R. R., and R. D. Hunsucker (1977), *J. Atmos. Terr. Phys., 39*, 487–501.
Henderson, M. G. (1994), PhD thesis, University of Calgary.
Henderson, M. G. (2009), *Ann. Geo.*, *27*(5), 2129–2140.
Heppner, J. P. (1954), *J. Geophys. Res., 59*, 329.
Heppner, J. P. (1958), DR135, Defence Research Board of Canada, Ottawa, Ontario.
Hiorter, O. P. (1747), *Kongle Swen Wetenskaps Acad Handlingar,* pp. 27–43.

Horton, W., et al. (2001), *J. Geophys. Res.*, *106*, 18803–18822; *96*, 11389–11401.
Jacobs, J. A, and K. Sinno (1960), *Geophys. J. Roy. Astron. Soc., 3*, 333–353.
Jacobs, J. A., et al. (1963), *J. Geophys. Res., 68*(14), 4373–4374.
Jacobs, J. A., et al. (1964), *J. Geophys. Res., 69*, 180.
Kataoka, R., et al. (2009), *J. Geophys. Res., 114*, A09202, doi:10.1029/2009JA014214.
Keiling, A, and K. Takahashi, (2011), *Space. Sci. Rev.*, *161*, 63–148
Kepko, L., and R. L. McPherron (2001), *J. Geophys. Res., 106*(A9), 18919–18922, doi:10.1029/2000JA000189.
Knudsen, D. J. (2001), *Geophys. Res. Lett., 28*, 705
Lee, L. C., et al. (1998), *J. Geophys. Res.*, *103*, 29419–29428.
Lessard, M. R., et al. (2006), *Geophys. Res. Lett., 33*, L14108, doi:10.1029/2006GL026411
Lester, M., et al. (1983), *J. Geophys. Res., 88*(A10), 7958–7966, doi:10.1029/JA088iA10p07958.
Lester, M., et al. (1984), *J. Geophys. Res., 89*(A7), 5489–5494, doi:10.1029/JA089iA07p05489.
Liang, J., et al. (2008), *Geophys. Res. Lett., 35*(17), L17S19.
Liou, K., and Y.-L. Zhang (2009), *J. Geophys. Res., 114*, A10206, doi:10.1029/2009JA014207.
Lui, A. T. Y., et al., (1991), *J. Geophys. Res.*, *96*(A7), 11389–11401, doi:10.1029/91JA00892.
Lysak, R. L. (1991), *J. Geophys. Res., 96*, 1553, doi:10.1029/90JA02154.
Lysak, R. L., and Y. Song (2008), *Geophys. Res. Lett., 35,* L20101, doi:10.1029/2008GL035728.
McPherron, R. L (1970), *J. Geophys. Res., 75*, 5592–5599.
McPherron, R. L. (1973), et al., *J. Geophys. Res.*, *78*, 3131–3149.
Mann, I.R., et al. (2008), *Space Sci. Rev.*, *141*, 413–451. doi:10.1007/s11214-008-9457-6
Matsushita, S. (1963), *J. Geophys. Res., 68*(14), 4369–4372.
Mende, S. B., et al. (2003), *J. Geophys. Res., 108*, 8010, doi:10.1029/2002JA009413, A4.
Mende, S. B., et al., (2008), *Space Sci. Rev.*, *141*, 357–387.
Meyer, Y. (1989), in *Wavelets* (eds. J. M. Combes, A. Grossmann, and Ph. Tchamitchian), pp. 21–37
Milling, D.K., et al., (2008), *Geophys. Res. Lett., 35*, L17S20, doi:10.1029/2008GL033672.
Morioka, A. et al., (2014), *J. Geophys. Res. 119*, 1044–1059, doi:10.1002/2013JA019442.
Murphy, K.R., et al., (2009a). *J. Geophys. Res.*, *114*(2), doi:10.1029/2008JA013548
Murphy, K. R., et al., (2009b), *J. Geophys. Res.*, *114*, A00C16, doi:10.1029/2008JA013548.
Murphy, K.R., et al., (2011), *J. Geophys. Res.*, *116*(1), doi:10.1029/2010JA015757
Murphy, K. R., et al. (2015), *J. Geophys. Res.*, *119*, 9684–9701. doi:10.1002/2014JA019795.
Nishimura, Y., et al., (2010), *J. Geophys. Res.*, *115*, A07222, doi:10.1029/2009JA015166.
Nose, M., et al. (1998), *Earth Planets Space*, *50*(9), 773–783
Ohtani, S.-I. (2004), *Space Sci. Rev., 113*, 77–96, doi:10.1023/B:SPAC.0000042940.59358.2f.
Olson, J. V., and G. Rostoker (1975), *Planet. Space Sci., 23*, 1129–1139
Partamies, N., et al. (2010), *Ann. Geo., 28*, 711
Perraut, S., et al. (2000), *J. Geophys. Res.*, *105*, 21097–21107.
Petrukovich, A. A., and A. G. Yahnin, *Space Sci. Rev.*, *122*, 81–87, doi:10.1007/s11214-006-7022-8, 2006.
Posch, J. L., et al. (2007), *J. Atmos. Solar-Terr. Phys., 69*(15), 1775–1796
Rae, I. J., et al. (2009a), *J. Geophys. Res.*, *114*(7), doi:10.1029/2008JA013771
Rae. I. J., et al. (2009b), *J. Geophys. Res.*, *114*(1), doi:10.1029/2008JA013559
Rae, I. J., et al. (2010), *J. Geophys. Res.*, *115*(10), doi:10.1029/2010JA015376
Rae, I. J., et al. (2011). *J. Geophys. Res.*, *116*(1), doi:10.1029/2010JA015762
Rae, I. J., et al. (2012), *J. Geophys. Res.*, *117*(8), doi:10.1029/2012JA017534
Roux, A. (1985), *Eur. Space Agency Spec. Publ.,* ESA SP-235, 151–159.
Roux, A., et al. (1991), *J. Geophys. Res.*, *96*, 17697–17714.
Russell, C. T., et al. (2008), *Space Sci. Rev.*, *141*, 389–412.
Saito, T. (1961), *Sci. Rep. Tohoku Univ. Set. 5,* 13, 53–61.
Saito, T. (1969), *Space Sci. Rev.*, *10*(3), 319–412
Sakaguchi, K., et al. (2009), *Ann. Geophys., 27*, 623–630.
Samson, J. C., et al. (1971), *J. Geophys. Res.*, *76*, 3675.
Samson, J. C. (1973), *Geophys. J. Roy. Astron. Soc., 34*, 403–419.
Samson, J.C. (1983), *Geophys. J. R. astron. Soc.*, *72*, 647–664.
Samson, J. C., et al. (1992a), *Geophys. Res. Lett., 19*, 2167–2170.
Samson, J. C., et al. (1992b), *J. Geophys. Res.*, *97*, 8495–8518.
Samson, J. C., et al. (1996), *J. Geophys. Res.*, *101*, 17373–17383.
Semeter, J., et al. (2005), *J. Geophys. Res., 110*, A11310, doi:10.1029/2005JA011226
Sibeck, D. G., and V. Angelopoulos (2008), *Space Sci. Rev*.
Troitskaya, V. A. *(*1961*), J. Geophys. Res., 66*, 5–18.
Trondsen, T. S (1997), *Geophys. Res. Lett.*, *24*, 2945.
Uritsky, V. M., et al. (2009), *Geophys. Res. Lett., 36*, L21103.
Voronkov, I., et al. (1999), *J. Geophys. Res., 104*(A12), 28491–28505, doi:10.1029/1999JA900362.
Voronkov, I. O., et al. (2000), *J. Geophys. Res., 105*, 18505–18518.
Voronkov, I. O., et al. (2003), *J. Geophys. Res.*, *108*, 1073, doi:10.1029/2002JA009314.
Wang, C.-P., et al. (2006), *J. Geophys. Res., 111*, A04215, doi:10.1029/2005JA011545
Walsh, A. P., et al. (2010), *J. Geophys. Res., 115*, A00I13, doi:10.1029/2010JA015748.
Watt, C. E. J., and R. Rankin (2009), *Phys. Rev. Lett.*, *102,* 045002.
Watt, C. E. J., and R. Rankin (2010), *J. Geophys. Res.*, *115*, A07224, doi:10.1029/2009JA015185.
Watt C. E. J., and R. Rankin (2012), in *Auroral Phenomenology and Magnetospheric Processes: Earth and Other Planets* (eds. A. Keiling, E. Donovan, F. Bagenal and T. Karlsson), American Geophysical Union, Washington, D.C. doi: 10.1029/2011GM001171.
Wygant, J. R., et al. (2000), *J. Geophys. Res., 105*, 18675–18692, doi:10.1029/1999JA900500.
Yoon, P. H., et al. (1996), *J. Geophys. Res., 101*, 27327–27339.
Yoon, P. H., et al. (1994), *Phys Plas.*, *1*, 3033–3043.
Zhu, Z. W., and R. M. Winglee (1996), *J. Geophys. Res, 101*, 4885–4897.